Aircraft noise exposure drives the activation of white blood cells and induces microvascular dysfunction in mice

Redox Biology 46 (2021) 102063

Contents lists available at ScienceDirect

Redox Biology

journal homepage: www.elsevier.com/locate/redox

Aircraft noise exposure drives the activation of white blood cells and induces microvascular dysfunction in mice

Jonas Eckrich [a,1], Katie Frenis [b,1], Giovanny Rodriguez-Blanco [c], Yue Ruan [d], Subao Jiang [d], Maria Teresa Bayo Jimenez [b], Marin Kuntic [b], Matthias Oelze [b], Omar Hahad [b,e], Huige Li [f], Adrian Gericke [d], Sebastian Steven [b,e], Sebastian Strieth [a], Alex von Kriegsheim [c], Thomas Münzel [b,e,**], Benjamin Philipp Ernst [a,1], Andreas Daiber [b,e,1,*]

[a] Department of Otorhinolaryngology, University Medical Center Bonn (UKB), Bonn, Germany
[b] Department of Cardiology, Cardiology I, University Medical Center Mainz, Mainz, Germany
[c] Institute of Genetics and Cancer, University of Edinburgh, UK
[d] Department of Ophthalmology, University Medical Center of the Johannes Gutenberg University Mainz, Germany
[e] German Center for Cardiovascular Research (DZHK), Partner Site Rhine-Main, Mainz, Germany
[f] Department of Pharmacology, University Medical Center of the Johannes Gutenberg University Mainz, Germany

ARTICLE INFO

Keywords:
Aircraft noise exposure
Inflammatory phenotype
Plasma proteome
Dorsal skinfold model
Microvascular dysfunction
Phagocytic NADPH oxidase

ABSTRACT

Epidemiological studies showed that traffic noise has a dose-dependent association with increased cardiovascular morbidity and mortality. Whether microvascular dysfunction contributes significantly to the cardiovascular health effects by noise exposure remains to be established. The connection of inflammation and immune cell interaction with microvascular damage and functional impairment is also not well characterized. Male C57BL/6J mice or gp91phox$^{-/y}$ mice with genetic deletion of the phagocytic NADPH oxidase catalytic subunit (gp91phox or NOX-2) were used at the age of 8 weeks, randomly instrumented with dorsal skinfold chambers and exposed or not exposed to aircraft noise for 4 days. Proteomic analysis (using mass spectrometry) revealed a pro-inflammatory phenotype induced by noise exposure that was less pronounced in noise-exposed gp91phox$^{-/y}$ mice. Using *in vivo* fluorescence microscopy, we found a higher number of adhesive leukocytes in noise-exposed wild type mice. Dorsal microvascular diameter (by trend), red blood cell velocity, and segmental blood flow were also decreased by noise exposure indicating microvascular constriction. All adverse effects on functional parameters were normalized or improved at least by trend in noise-exposed gp91phox$^{-/y}$ mice. Noise exposure also induced endothelial dysfunction in cerebral microvessels, which was associated with higher oxidative stress burden and inflammation, as measured using video microscopy. We here establish a link between a pro-inflammatory phenotype of plasma, activation of circulating leukocytes and microvascular dysfunction in mice exposed to aircraft noise. The phagocytic NADPH oxidase was identified as a central player in the underlying pathophysiological mechanisms.

1. Introduction

Epidemiological studies showed that traffic noise has a dose-dependent association with increased cardiovascular morbidity and mortality [1,2]. According to the WHO guidelines, the pooled relative risk for ischemic heart disease (IHD) was 1.08 (95% CI 1.01–1.15) per 10 dB(A) increase in noise exposure, starting at 50 dB(A). A large proportion of the population (more than one third in Europe) is exposed to noise levels exceeding the guidelines. The WHO also estimates that at least 1.6 million healthy life years are lost annually from traffic-related noise in Western Europe [3]. The latter estimation is supported by a recent study in Switzerland concluding that loss of healthy life years due to traffic are dominated by air pollution, whereas morbidity/indicators of life quality are dominated by noise [4]. Traffic noise at night causes

* Corresponding author. University Medical Center Mainz, Center for Cardiology, Cardiology I, Geb. 605, Langenbeckstr. 1, 55131, Mainz, Germany.
** Corresponding author. University Medical Center Mainz, Center for Cardiology, Cardiology I, Geb. 605, Langenbeckstr. 1, 55131, Mainz, Germany.
E-mail addresses: tmuenzel@uni-mainz.de (T. Münzel), daiber@uni-mainz.de (A. Daiber).
[1] Means equal contribution – joint first or senior authors.

https://doi.org/10.1016/j.redox.2021.102063
Received 25 May 2021; Received in revised form 3 July 2021; Accepted 5 July 2021
Available online 8 July 2021

fragmentation and shortening of sleep, elevation of stress hormone levels, and increased oxidative stress in the vasculature and the brain [5]. These factors can promote vascular dysfunction (endothelial dysfunction) and hypertension, thus elevating cardiovascular risk [6]. Chronic exposure to transportation noise (railway and road traffic) was also associated with an increase in arterial stiffness in the general population [7] and acute (one night) exposure to aircraft noise caused endothelial dysfunction in healthy subjects [8], both accepted subclinical markers of atherosclerosis and development of future cardiovascular disease [9]. Noise also decreased pulse transit time, reflecting sympathetic activation, in healthy subjects [8].

From a mechanistic view, noise exposure activates neuronal stress response pathways that are characterized by the release of stress hormones such as catecholamines and cortisol (corticosterone in rodents) [8,10–12]. The circulating stress hormones, also via interaction with other endocrine systems such as the renin-angiotensin-aldosterone and endothelin-1 systems [13], lead to enhanced vasoconstriction as well as vascular inflammation and oxidative stress, all of which contributes to endothelial dysfunction and higher blood pressure [14,15]. Whereas the impact of noise exposure on large vessels is well characterized in animals [14–16] and humans [8,17], adverse effects of noise on the peripheral microvascular function are almost completely unaddressed, but for one study in mesenteric arteries [18] and many studies on a role of cochlear microvascular damage in hearing loss [19]. This represents a clear gap in actual noise research, especially as the observed blood pressure increases by chronic noise exposure in primates [20] as well as loss of mesenteric microvascular integrity (enhanced leakiness) in laboratory animals exposed to loud noise [21] can be best explained by noise-dependent microvascular dysfunction.

As the effects of noise on microvascular function and its link to vascular inflammation are not sufficiently characterized, we investigate with the present study the impact of noise on pro-inflammatory changes of the plasma proteome, the interaction (rolling) of white blood cells with the microvasculature and microvascular function in a model of dorsal skinfold chamber instrumented mice.

2. Methods

2.1. Animals

For *in vivo* experimentation, male C57BL/6j (wt) or gp91phox$^{-/y}$ mice, aged > 8 weeks (>25 g body weight) were used as an experimental model. A total number of 37 mice were used: 9 for proteomics, 20 for dorsal skinfold chamber, including mice for setup of the model, and 8 for cerebral microvessels). All experimental procedures were performed according to institutional and governmental guidelines and all people involved in the experimental course were qualified to perform experimental procedures on laboratory animals (FELASA B/C accreditation). All animal experiments were approved by the Landesuntersuchungsamt Koblenz, Germany (23 177-07/G 18-1-084 and addenda). For the surgical procedures, animals were anesthetized by intraperitoneal injection of ketamine (0.1 mg/g Ketanest; Pfizer Pharma GmbH, Berlin, Germany) and xylazine (0.01 mg/g Rompun; Bayer, Leverkusen, Germany). After chamber implantation, weight and health conditions of every animal were monitored and documented in a score sheet quantifying indicators of impaired wellbeing. A weight loss >20% of the postoperative bodyweight, signs of inflammation and behavioral changes indicating pain or sickness as well as signs of inflammation within the chamber window were determined as dropout criteria.

2.2. Dorsal skinfold chamber preparation

After sufficient anesthesia was determined by a loss of positional as well as corneal and interdigital reflexes, the surgical procedure was carried out as previously described [22]. After mechanical and chemical depilation with an electric razor (Remington Contour, Spectrum Brands, Middleton, Wisconsin, USA) and depilatory cream (Veet, Reckitt Benckiser Deutschland GmbH, Heidelberg, Germany) two antagonizing sides of a titanium frame were sutured onto a double layer skinfold of the anesthetized animal (Fig. 1). Both chamber frames were screwed together with sweeping screws. In the area of the chamber window the skin as well as the underlying musculocutaneus tissue was surgically removed. A cover glass slip (11.8 mm, Hecht Assistant, Glaswarenfabrik Karl Hecht GmbH & Co KG, Sondheim, Germany) was subsequently placed on the musculocutaneous tissue of the opposing layer within the chamber window and fixed with a retaining ring. For postoperative analgesia, the animals received 0.1 mg/mL tramadol (Tramadol-ratiopharm, ratiopharm GmbH, Ulm, Germany) within the daily applied drinking water.

2.3. Noise exposure

Before surgical procedures, animals had previously been assigned to the noise exposure or sham control groups (noise/control). Subsequently, after recovery from the chamber preparation, the animals were either exposed to a previously-recorded playback of aircraft noise (average sound pressure level of 72 dB(A) and peak sound pressure levels of 85 dB(A), respectively) for 96 h or kept at homologous conditions without noise exposure (mean background noise levels in the animal house were approximately 48 dB(A)) as previously described [14,15]. After chamber preparation, animals of either group were isolated and had free access to tap water as well as normal food (ssniff, Spezialdiaeten GmbH, Soest, Germany) throughout the entire course of the experiment. For dorsal skinfold chamber experiments, two groups per genotype (wt or gp91phox$^{-/y}$) were investigated: a control group with only the dorsal skinfold chamber (sham) and a group with the chamber and 4 days of noise exposure (noise). For plasma proteome analysis and cerebral arteriole functional studies, no chamber was implanted and only two groups were studied: wt and noise.

2.4. Plasma proteome analysis

2 µl of plasma were resuspended in 10 µl 6 M guanidium HCl, 100 mM Tris pH8.5, 10 mM tris(2-carboxyethyl)phosphine, 15 mM chloracetamide and heated to 95 °C for 5 min 1 µg of LysC (Wako, Japan) was added and the sample was digested for 4 h at 37 °C. Sample was diluted 6x with water and 1 µg of porcine trypsin was added (Promega, Southampton, UK). Digest was continued overnight at 37 °C. Peptides were desalted using Stagetips as described [23]. Peptides were labelled using TMTpro (Thermo Fisher, Abingdon, UK) according to the manufacturer's instructions. 15 TMT-labelled samples were combined and

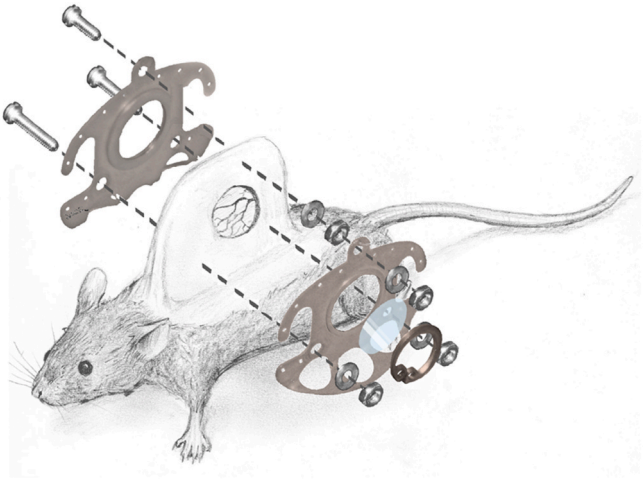

Fig. 1. Surgical anatomy and technical equipment of the dorsal skinfold chamber in mice.

fractionated into 12 fractions using high pH C_{18} reverse-phase ultra-high performance liquid chromatography (uHPLC) [24] on a 15 cm 2.1 mm, 1.7 μm BEH column (Waters, Elstree, UK) using gradients suggested by Thermo Fisher. 1 μg of the peptides were analyzed on a Fusion Lumos mass spectrometer coupled to and RSLCnano HPLC system (both Thermo Fisher). Peptides were separated using a 90-min gradient over an Aurora column (IonOptiks, Melbourne, Australia). Raw files were analyzed using the MaxQuant software suite [25]. Differential analysis was conducted using Perseus [26]. Briefly, the corrected reporter ion intensities were log2 transformed, normalized by median-subtraction and statistically relevant changes between the treatment groups identified by using permutation-based FDR determination. Clustering and String-network analysis was done using Cytoscape [27].

Alternatively, the digested peptides were analyzed using a Data-independent-acquisition (DIA) workflow. 2 μg of the peptides were analyzed on a Fusion Lumos mass spectrometer coupled to and RSLCnano HPLC system (both Thermo Fisher). Peptides were separated using a 150-min gradient over an Aurora column (IonOptiks, Melbourne, Australia). Acquisition parameters were copied from Ref. [28], briefly a MS window (350-1650 Da) was acquired at 120k resolution, followed by 46 MS/MS windows at 35k resolution covering 350-1650 Da of varying size with 1 Da overlap. Data was analyzed using Spectronaut 15 (Biognosis, Zurich, Switzerland) in directDIA mode using standard setting and searching against the Mouse Uniprot database. Ratios and standard error depicted were taken from the candidates.tsv output file generated by Spectronaut.

2.5. Metabolomics

Metabolites in plasma samples were extracted using three different monophasic extraction in a dilution of 1:4. Polar metabolites were extracted with 100% acetonitrile, whereas semipolar and lipid metabolites were extracted with 100% methanol and 100% isopropanol, respectively [29]. 20 μL of plasma were precipitated with the solvents and after overnight incubation at −80 °C, samples were centrifuged at 15 000 rpm, and the clear supernatant was transferred to clean HPLC vials prior to liquid chromatography-mass spectrometry (LC-MS) analysis.

Metabolite analysis was performed as described in Refs. [29,30]. In summary, we used a pHILIC column (Merck, Germany) to separate polar metabolites, and a Luna C_{18} (Phenomenex, United States) to separate non-polar metabolites. An Ultimate 3000 HPLC (Thermo Fisher Scientific, Germany) coupled to a Q-Exactive Orbitrap mass spectrometer (Thermo Fisher Scientific), which was operated in polarity switch mode, was used. Pooled plasma samples, chemical standards and procedure blanks were also analyzed along the chromatographic runs. Detailed descriptions of the methods are included in references in Refs. [29–31].

Lipid metabolites in plasma samples were analyzed using a nano-LC-MS/MS methodology described in Ref. [32]. We used an Aurora C_{18} column (IonOptics, Australia), and isopropanol-extracted samples were evaporated to dryness and reconstituted in a buffer containing 69% H_2O, 23% IPA and 8% BuOH and 5 mM H_3PO_4 [32].

Peak detection and integration from raw data were performed using Compound Discoverer 3.0 (Thermo Fisher Scientific) and also with XCMS [33]. Pathway enrichment of metabolite data was performed using the online tool mummichog [34] and the XCMS matrix as the input file. Lipidomics samples were analyzed using LipoStar software [35] and MS2 files were searched against LipidBlast database using LipiDex software [36].

2.6. Dot blot analysis of protein modification and expression in plasma samples

One μl of plasma protein (approximately 30 μg of protein) was transferred into each well to deposit on the nitrocellulose membrane (Sigma Aldrich, WHA10402506) via a Minifold I vacuum Dot-Blot system (Schleicher&Schuell, 10484138CP) [14,15], washed twice with 200 μl of PBS then dried for 60min at 60 °C to adhere the proteins. The membranes were then cut and incubated in Ponceau S solution (Sigma, P7170) for protein visualization and later normalization of the antibody staining. The stain was removed and the membrane blocked for 1 h at room temperature with 5% milk in PBS-T. The membranes were incubated with antibodies against caspase-3 (Cell Signaling, #9662S, 1:1000), thioredoxin interacting protein (TXNIP, Cell Signaling #14715, 1:1000), high-mobility-group-protein B1 (HMGB1, Cell Signaling #3935S, 1:1000), protease-activated receptor-1 (PAR1, BD Bioscience BD611522, 1:750), fibrinogen (Abnova #PAB5139 1:750) overnight at 4 °C. Positive bands were detected using ECL development (Thermo Fisher, 32 106, Millipore, ab5605, 1:750) and Chemilux Imager (CsX-1400 M, Intas). Densitometric quantification was performed using ImageJ software.

2.7. In vivo microscopy for analysis of microvascular reactivity and leukocyte interactions

Prior to the *in vivo* microscopy, fluorescein isothiocyanate (FITC)-labelled dextran (Sigma, Deisenhofen, Germany; average mol wt 500 000; 0.5–0.75 mL of a 5% solution in 0.9% saline) and rhodamine 6G (Sigma, Deisenhofen, German 0.5-0,75 mL of a 0.05% solution in 0.9% saline) were injected in the tail veins in local anesthesia (Emla® 25 mg/g Lidocain +25 mg/g Prilocain creme, Aspen Germany GmbH, Munich, Germany). While FITC-labelled dextran was injected to enhance the contrast between plasma and blood cells in order to determine the specific blood flow, rhodamine 6G was administered to visualize leukocyte-endothelial cell interactions.

For the *in vivo* microscopy the animals were immobilized and placed in an acrylic glass tube and the chamber positioned horizontally underneath the microscope (Olympus BXFM, Olympus Deutschland GmbH, Hamburg, Germany) (Fig. 2). Since no invasive intervention was performed, no anesthesia was administered. After immobilization of the chamber, 5 regions of interest (ROI) within the chamber window (north, east, south, west, middle) were investigated and representative video sequences of each ROI were recorded using both a green filter (Excitation [Ex]:470 nm/Emission [Em]: 525 nm) as well as an orange filter (Ex: 545 nm; Em: 605 nm). ROIs were excluded if sufficient imaging was impossible due to non-adherence of the musculocutaneous tissue to the chamber window. The video sequences were processed using Cell Sens Dimension (Olympus Deutschland GmbH, Hamburg, Germany) and exported as uncompressed avi-files that were further processed to size-reduced mp4-files.

Off-line analysis was carried out using Cap Image (Dr. Zeintl Ingenieurbüro, Heidelberg, Germany) as previously described [37]. In each included ROI, vessel diameters, and blood flow velocities were

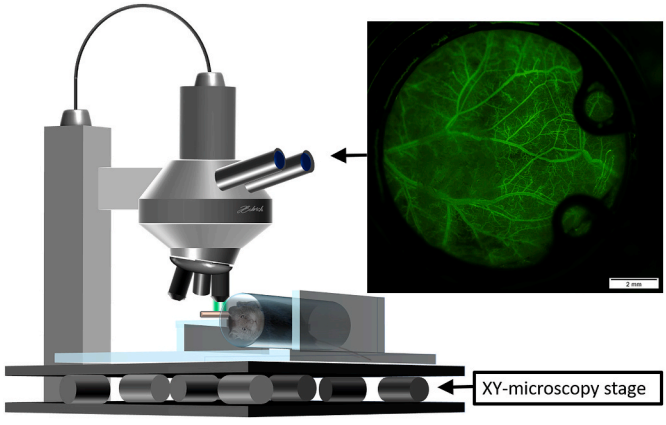

Fig. 2. Setup of fluorescein based *in vivo* microscopy of the dorsal skinfold chamber in mice.

determined and the segmental blood flow was calculated. To determine blood volume flowing through analyzed vessels over a given time, segmental blood flow q (in pl/s) was calculated as previously described by Baker and Wayland using the microvascular diameter (d) and red blood cell velocity (c): $q=(v/1.6)\ x\ (d/2)^2\ x\ \pi$ [38]. Furthermore, leukocyte-endothelial cell interactions were characterized by quantification of adherent cells as well as rolling (<50% of red blood cell velocity) cells crossing through a previously determined vascular segment.

2.8. Cerebral microvascular reactivity and oxidative stress

Microvascular reactivity was measured *in vitro* in arterioles branching from the middle cerebral artery (MCA) by using video microscopy as previously described for retinal and mesenteric microvessels with minor modifications [39–41]. After dissection, brains were transferred into ice cold artificial cerebrospinal fluid (aCSF) for preparation. Then, a vascular tree of the MCA was isolated and cleaned from surrounding tissue by using fine-point tweezers and Vannas scissors. Next, a micropipette was inserted into the lumen of the MCA and advanced into an arteriole branching from the main artery by using the lumen as a guide channel. Once the micropipette tip was placed in the lumen of the arteriole, the vessel was tied to the pipette with 10.0 nylon suture material, and the other end of the arteriole was tied to another micropipette. Subsequently, the arteriole was pressurized to 40 mmHg via the micropipette, visualized under brightfield conditions, and equilibrated for 30 min. Next, concentration-response curves for the thromboxane mimetic, U46619 (10^{-11} to 10^{-6} M; Cayman Chemical, Ann Arbor, MI, USA), were conducted. For measurement of vasodilation responses, vessels were then preconstricted to 50–70% of the initial luminal diameter by titration of U46619 and responses to the endothelium-dependent vasodilator, acetylcholine (ACh, 10^{-9} to 10^{-4} M; Sigma-Aldrich, Taufkirchen, Germany) and to the endothelium-independent nitric oxide donor, sodium nitroprusside (SNP, 10^{-9} to 10^{-4} M, Sigma-Aldrich), were determined. ROS formation was measured in cerebral arterioles branching from the MCA in 10 μm cryosections of the brain by dihydroethidium (DHE, 1 μM)-derived fluorescence (518 nm/605 nm excitation/emission), as previously described [41–43].

2.9. Immunohistochemistry of brain sections

Procedure for immunohistochemistry has been previously described [14,15,44]. Briefly, the right part of the brain was fixed in 4% formaldehyde, embedded in paraffin, and sliced into sections of 5 μm. Following deparaffinization, samples were blocked with normal horse blocking solution (Vector) and stained with a primary antibody against 3-nitrotyrosine (1:150, Merck-Millipore, Darmstadt, Germany). The biotinylated secondary antibody (Thermo Fisher Scientific, Waltham, MA, USA) was used at a dilution 1:1000. For immunochemical detection ABC reagent (Vector) and then DAB reagent (peroxidase substrate Kit, Vector) were used as substrates, then imaged with Cell Sens (Olympus).

2.10. Data management and statistical analysis

To compare *in vivo* microscopy findings, Mann-Whitney-U test for independent samples was applied. For comparison of vessel dose-response curves, 2-way ANOVA with Sidak's multiple comparison was used. Unpaired t-tests were used for targets identified by proteome analysis (Fig. 4), dot blot analysis (Fig. 5) and DHE measurements of cerebral microvessels (Fig. 8). Data of *in vivo* microscopy are expressed as the median and interquartile range while all other data are expressed as mean ± SD. Statistical analysis was performed using GraphPad Prism 9 (La Jolla, California, USA).

3. Results

3.1. Plasma proteome and metabolome analysis

To determine the systemic effects of noise stress on mouse physiology, blood plasma was isolated from 5 animals exposed to 96 h of aircraft noise and 4 untreated control animals. Plasma proteins were lysed, digested and labelled with isotopic peptide tags. This labelling strategy enables multiplexing and can resolve even subtle protein concentration changes in the plasma proteome. Overall, over 750 protein groups were quantified across the 9 plasma proteomes. 12 proteins were downregulated whereas 63 were upregulated by noise. Network analysis identified several clusters of connected proteins that were induced in blood plasma in the noise-treated group (Fig. 3a and b). Inspection of these clusters revealed that proteins regulating immunity and involved in the acute-phase response were upregulated, as well as other indicators of inflammatory and oxidative stress. We detected increased blood plasma levels of Saa1, Saa4, fibrinogen, complement factors and Reg3g, all of which are acute-phase proteins indicative of inflammation [45] (Fig. 4a). Moreover, we detected increased levels of the type I interferon receptor (Ifnar2) and of circulating gelsolin, suggesting engagement of the innate immune mechanism [46] (Fig. 4b). Furthermore, the increase of the cellular tight-junctions protein E-cadherin (Cdh1) is indicative of tissue leakage due to damage and proteolytic cleavage [47] (Fig. 4c). In addition, upregulation of the plasma glutathione peroxidase (Gpx3) is indicative of systemic oxidative stress [48] (Fig. 4d). Oxidative stress appears to have left an imprint on the metabolome as well. We found that plasma levels of unsaturated fatty acids were reduced upon noise stress, whereas concentrations of the corresponding saturated fatty acids were not changed (Fig. 4e). This reduction is indicative of lipid peroxidation and is a surrogate of oxidative stress [49,50].

Taken together these data suggests that noise stress induces systemic inflammation, oxidative stress and, possibly as a consequence, tissue damage. Moreover, the enhanced expression of integrin binders, such as vitronectin and fibrinogen (Fig. 3a), would suggest altered adhesion dynamics of circulating platelets and immune cells.

Immunological screening by dot blot analysis revealed that the noise-induced changes of selected markers of inflammation or oxidative stress show less pronounced increases in exposed gp91phox$^{-/y}$ as compared to C57BL/6J (wt) mice (Fig. 5a), which is in accordance with the less pronounced proteomic changes in the plasma of noise-exposed gp91phox$^{-/y}$ mice (Fig. 5b).

3.2. In vivo microscopy of dorsal skinfold chambers

C57BL/6J (wt) as well as gp91phox$^{-/y}$ mice were randomized to be exposed to around-the-clock aircraft noise for 96 h (noise) or sham control group (control) with no noise exposure. Subsequently, fluorescein-based measurements were carried out to determine noise-induced effects on microcirculatory parameters and leukocyte-endothelial interactions *in vivo*.

3.3. Noise-induced effects on leukocyte-endothelial interaction in vivo

Rhodamine 6G based *in vivo* microscopy showed a significantly increased number of adhesive leukocytes (12.25 vs. 1.25 n/ROI, $p = 0.0286$) within the analyzed microvessels following aircraft noise exposure when compared to sham control in wt mice (see Fig. 6a and **suppl. video file 1&2**). This was not reproduced in noise exposed gp91phox$^{-/y}$ mice which had equal numbers of adhesive leukocytes (2.25 vs. 2.5 n/ROI, $p > 0.9999$, see Fig. 6a and **suppl. video file 3&4**). Rolling leukocytes did not differ significantly between noise exposed wt (6.3 vs. 2.67, $p = 0.6857$) and gp91phox$^{-/y}$ (5.0 vs. 2.75 n/ROI, $p = 0.7$) mice and sham controls (see Fig. 6b).

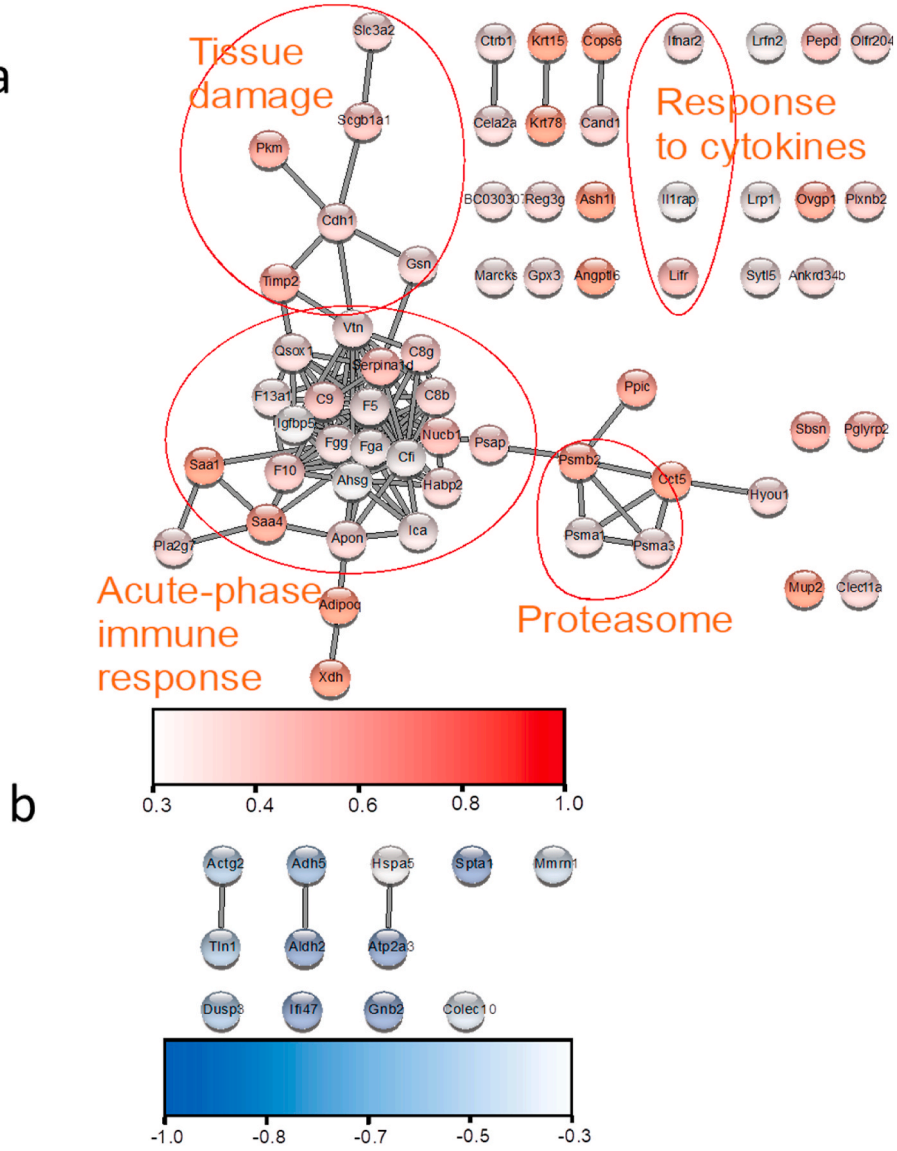

Fig. 3. Network analysis of blood plasma proteins that are significantly regulated by 96 h of aircraft noise exposure. (a) Induced protein group in several clusters indicative of systemic inflammation and tissue damage. (b) On the other hand, no prominent clusters of downregulated markers were recognized. The data are mean of n = 4–5 mice per group.

3.4. Noise-induced effects on microcirculation in vivo

Comparative analysis of microcirculatory analysis using FITC-dextran based *in vivo* microscopy revealed a significantly reduced red blood cell velocity (0.22 vs. 0.86 mm/s, p = 0.0286) with consecutive reduced segmental blood flow (36.45 vs. 405.95 pl/s, p = 0.0286) in wt mice following aircraft noise exposure when compared to sham controls (see Fig. 7b and c and **suppl. video file 5&6**). In contrast, red blood cell velocity (0.17 vs. 0.32 mm/s, p = 0.2, see Fig. 7a) and segmental blood flow (82.4 vs. 136.77 pl/s, p = 0.7) were not significantly impaired by aircraft noise exposure in gp91phox$^{-/y}$ mice (see Fig. 7b and c and **suppl. video file 7&8**) compared to sham controls. Blood vessel diameters did not differ significantly between investigative groups and sham controls (although a minor decrease by trend was noticed), neither in wt nor in gp91phox$^{-/y}$ mice (see Fig. 7a).

Cerebral microvessel function was measured using video microscopy to investigate the vasodilative and vasoconstrictive behavior of the vessels following noise exposure. Responses to endothelium-dependent vasodilation via acetylcholine were significantly impaired following 96h of noise exposure and even resulted in paradoxical constriction, indicative of damage to the endothelium (46.8% vs −17.4% change in diameter at maximum). Smooth muscle-dependent vasorelaxation via nitroprusside and constriction via thromboxane A2 receptor agonist U46619 appeared to be unaffected by noise exposure (Fig. 8a). Correspondingly, ROS levels within the cerebral arterioles of noise-exposed wt mice were significantly increased (211%) from unexposed counterparts, as measured by DHE staining (Fig. 8b). In support of the higher burden of nitro-oxidative stress, the level of 3-nitrotyrosine-positive proteins was increased by noise in brain sections as revealed by immunohistochemistry (Fig. 8c).

4. Discussion

Our present data demonstrate that aircraft noise exposure for 4 days leads to a pro-inflammatory phenotype of the plasma proteome and enhanced interaction of white blood cells with the microvasculature in wt but not in gp91phox$^{-/y}$ mice. The number of adhesive leukocytes was increased in noise-exposed wild type mice (the number of rolling leukocytes by trend), all of which was prevented by genetic deletion of gp91phox, the phagocytic NADPH oxidase. In addition, microvascular

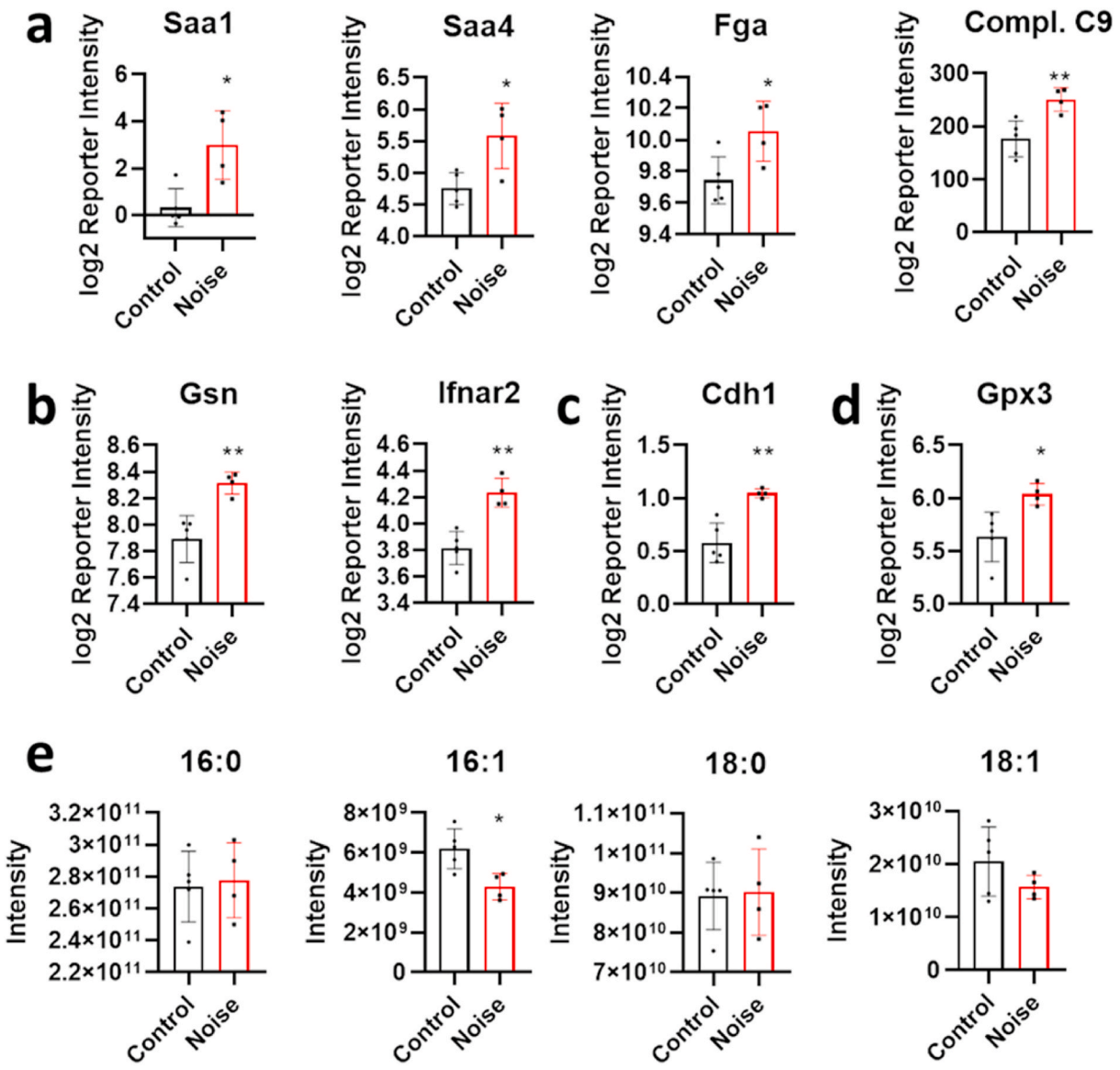

Fig. 4. Comparative proteomic analysis of blood plasma from C57BL/6J either control treated or following around-the-clock aircraft noise exposure for 96 h. (a) Induction of acute-phase proteins or (b) markers of the activation of innate immunity. (c,d) Additionally, the detection of the tight-junction protein E-cadherin and the extracellular glutathione peroxidase Gpx3. (e) The relative reduction of unsaturated fatty acids is also a hallmark of oxidative stress. The data are mean ± SD of n = 4–5 mice per group. *, $p < 0.05$ vs. Control; **, $p < 0.01$ vs. Control.

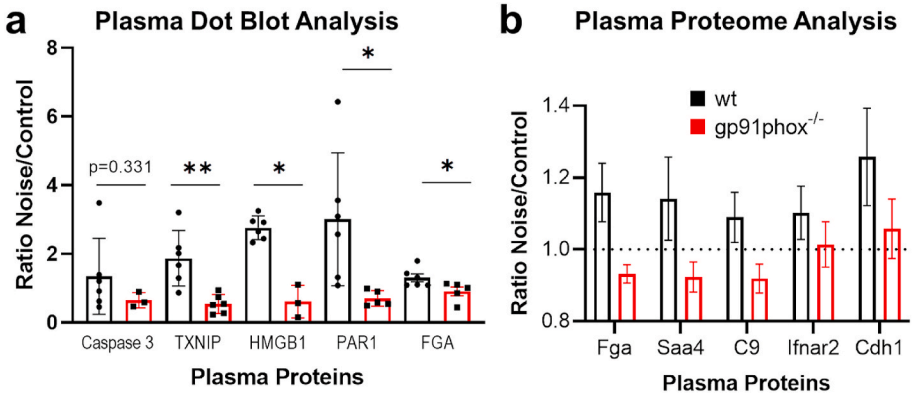

Fig. 5. Comparative dot blot and proteome analysis of blood plasma from C57BL/6J or gp91phox$^{-/y}$ mice either control treated or following around-the-clock aircraft noise exposure for 96 h. (a) Ratio for plasma levels of caspase-3, thioredoxin interacting protein (TXNIP), high-mobility-group-protein B1 (HMGB1), protease-activated receptor-1 (PAR1) and fibrinogen (FGA) in noise exposed versus unexposed (control) animals by dot blot analysis. Ratios were calculated by pairing the lowest or highest signals in the noise-exposed and unexposed animals. The data are mean ± SD of n = 3–6 plasma samples per group. *, $p < 0.05$ vs. Control; **, $p < 0.01$ vs. Control. (b) Induction of plasma proteins as determined by DIA mass spectrometry in control versus noise stressed animals (Saa4, serum amyloid A4; C9, complement component 9; Ifnar2, interferon alpha and beta receptor subunit 2; Cdh1, cadherin 1). Ratios depicted as determined by Spectronaut (only significantly different targets are shown, based on the target profile depicted in Fig. 4), error bars are SEM. n = 4–6 animals.

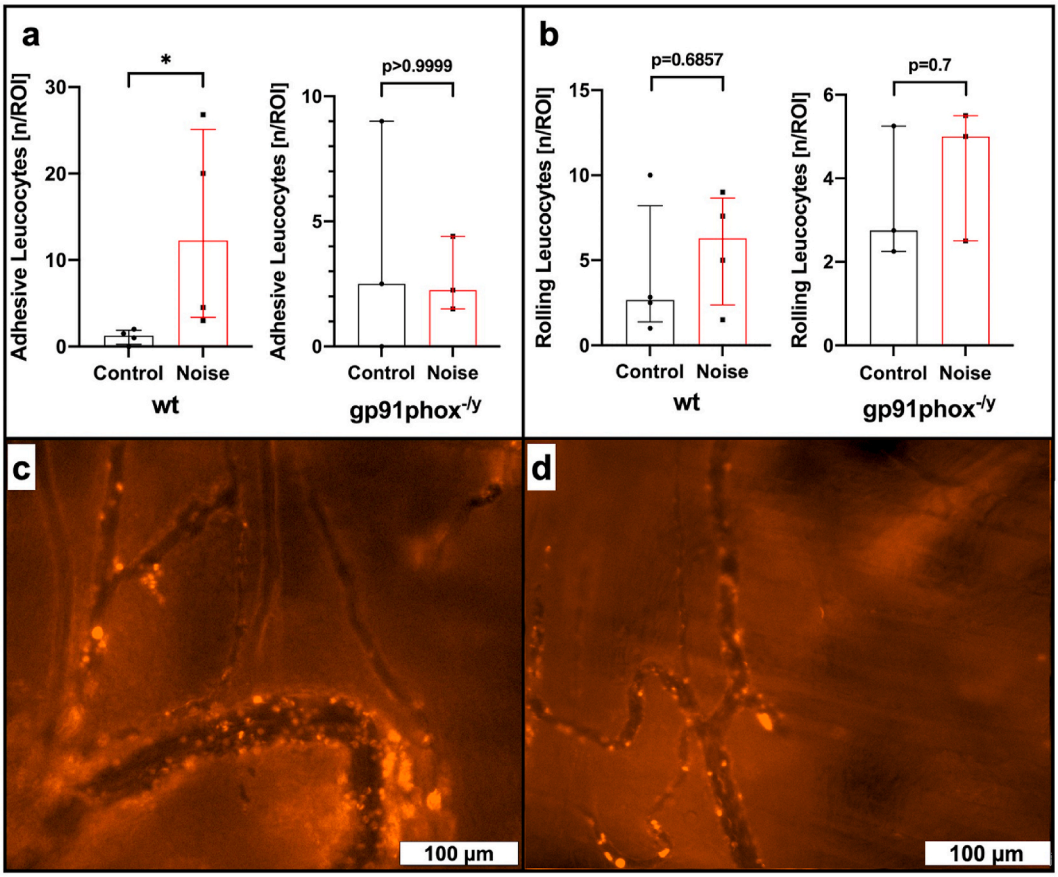

Fig. 6. Effects of noise on leukocyte-microvascular wall interactions. Rhodamine 6G based *in vivo* microscopy shows a significant increase in adhesive leukocytes within analyzed microvessels in C57BL/6J wild type (wt) mice following around-the-clock aircraft noise exposure for 96 h (a). This effect was not observed in gp91phox$^{-/y}$ mice (a). Additionally, aircraft noise had no significant impact on rolling leukocytes, neither in wt nor in gp91phox$^{-/y}$ mice (b). Exemplary images of rhodamine 6G based imaging of leukocyte-endothelial interaction in noise exposed wt (c) and gp91phox$^{-/y}$ (d) mice. Data are reported as the median and interquartile range of n = 4 (wt) or 3 (gp91phox$^{-/y}$ animals per group and per animal n = 3–4 independent measurements were carried out. *, $p < 0.05$ vs. sham control (Control).

diameter (by trend), red blood cell velocity and segmental blood flow were decreased by noise exposure indicating microvascular constriction. These markers of microvascular dysfunction were largely improved in gp91phox knockout mice. With our present data, we establish a link between a pro-inflammatory milieu, activation of circulating leukocytes and microvascular dysfunction in mice exposed to aircraft noise with a central role of the phagocytic NADPH oxidase in the underlying pathophysiological mechanisms.

According to the noise-stress-concept proposed by Babisch [11], noise initiates neuronal stress responses via indirect pathways such as annoyance, anxiety but also impairment of sleep quality leading to increased levels of stress hormones that become manifest in cardiovascular disease, including acute MI, heart failure, hypertension, arrhythmia and stroke [6,51]. This sequence of events is supported by human data demonstrating activation of the amygdala by noise, which is associated with increased coronary atherosclerotic inflammatory changes and higher incidence of major adverse cardiovascular events (MACE) as revealed by molecular insights using positron emission tomography scanning [52]. A perturbation of the autonomic nervous system, and/or sympatho-adrenal activation [53,54], the release of pro-inflammatory mediators, modified lipids or phospholipids and activation of leukocyte populations, endothelial dysfunction and activation of pro-thrombotic pathways are crucial for noise-triggered cardiometabolic diseases [6,55].

In a field study, we demonstrated that night-time aircraft noise exposure (mean sound pressure level [L_{eq}] 46.3 dB(A), peak level 60 dB (A) for one night) reduced sleep quality and increased stress hormone levels. Endothelial dysfunction in response to aircraft noise exposure for one night was also more pronounced in patients with coronary artery disease [56] than in healthy subjects [8]. Importantly, co-treatment with the antioxidant vitamin C largely improved noise-induced endothelial dysfunction pointing to an essential role of oxidative stress. Endothelial dysfunction in healthy subjects exposed to train noise was also associated with an inflammatory, pro-oxidative and pro-thrombotic phenotype of the plasma proteome [17]. Recent animal studies (L_{eq} 72 dB(A), peak level 85 dB(A) for 24 h/d for 1, 2 and 4 d) revealed an essential role of oxidative stress, enhanced inflammatory signaling, impairment of the circadian clock and dysregulation of gene networks leading to endothelial dysfunction, and vascular/cerebral damage from aircraft noise [14,15]. Endothelial dysfunction, enhanced inflammation and infiltration of immune cells into the vasculature (revealed by aortic FACS analysis) represent early hallmarks of noise exposure in mice [14] that were mostly prevented by genetic deletion of Nox2 (gp91phox) [15], but aggravated in the presence of pre-existing arterial hypertension in mice [44]. Of note, uncoupling of eNOS, a major trigger of endothelial dysfunction, was prevented in Nox2 (gp91phox) knockout mice, indicating phagocyte-derived oxidative stress as an important contributor to the detrimental cardiovascular effects observed following acute noise exposure [15].

Previous translational studies were primarily focused on effects of noise in conductance vessels and the brain, with the blood serving as an intermediary, which propagates vessel dysfunction. In the present study, we aimed to assess the effects of noise within the microcirculation, which has not been previously addressed. Our data using video

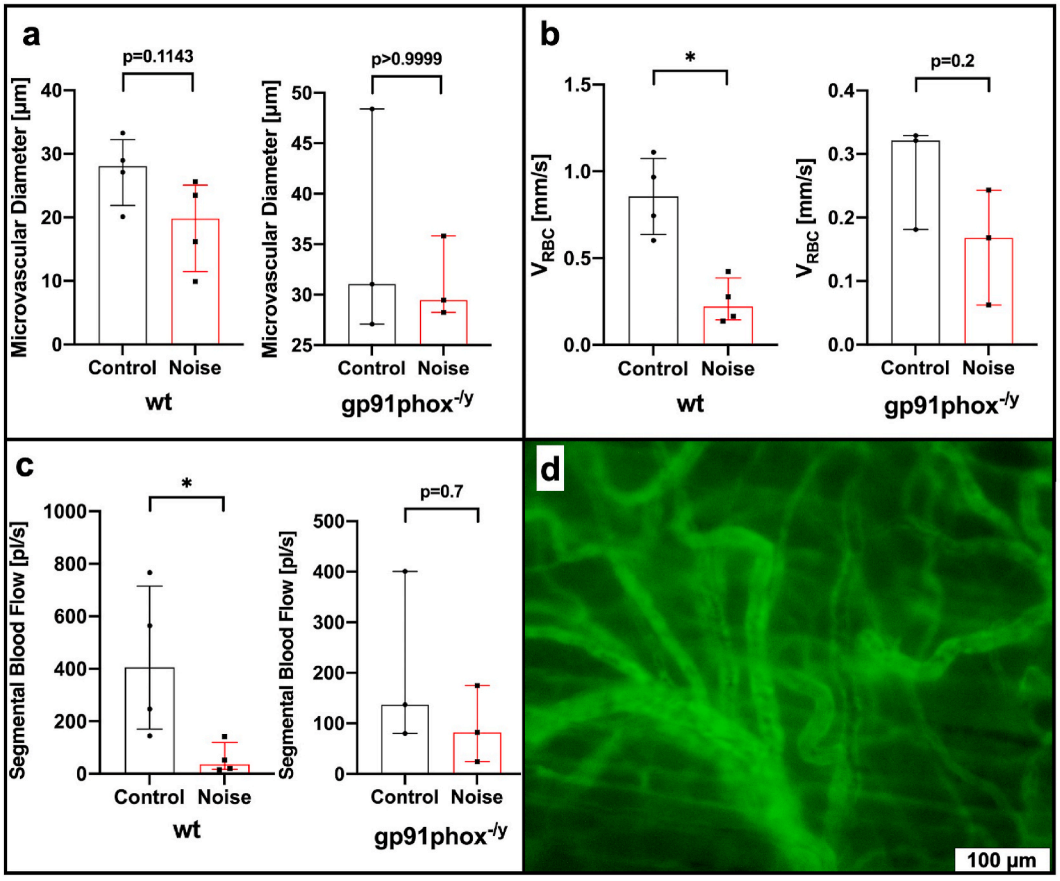

Fig. 7. Effects of noise on microvascular diameter, red blood cell velocity and segmental blood flow. FITC-dextran based *in vivo* microscopy (d) reveals no significant changes in microvascular diameter in C57BL/6J wild type (wt) or gp91phox$^{-/y}$ mice following around-the-clock aircraft noise exposure for 96 h (a). In contrast, red blood cell velocity (V_{RBC}, b) as well as segmental blood flow (SBF, c) were significantly reduced in noise exposed wt mice. This was not reproduced in gp91phox$^{-/y}$ mice where no significant changes were observed. Data are reported as median and interquartile range n = 4 (wt) or 3 (gp91phox$^{-/y}$) animals per group and per animal n = 3–4 independent measurements were carried out. *, $p < 0.05$ vs. sham control (Control). (For interpretation of the references to colour in this figure legend, the reader is referred to the Web version of this article.)

microscopy of cerebral microvessels demonstrated a profound dysfunction of endothelium-dependent vasodilation, but not smooth muscle-mediated vascular function. Endothelial dysfunction is widely reported in conductance vessels in cardiovascular disease in humans [57,58] and rodents [59,60], but data within microvessels is sparser, especially in the context of environmental stressors, although coronary microvascular function was proposed as an important target for cardioprotection [61]. Our data reveal a sensitivity of cerebral microvessels to stress responses, in line with our recently published study demonstrating improvement of microvessel function following leukocyte ablation [41]. Alongside these findings, we herein report that the number of leukocytes adhered to the endothelium of wild type microvessels was significantly increased, while this behavior was not present in the noise-exposed gp91phox$^{-/y}$ genotype, indicating that reactive oxygen species (ROS) derived from phagocytes are a critical component in the endothelial damage found in vessels following noise exposure. We did not find significant differences in the number of rolling leukocytes in either genotypes. However, rolling represents a low-affinity behavior, whereas adhesion, a parameter significantly increased in only wild type noise-exposed mice and normalized in gp91phox$^{-/y}$, is a committed step in the *trans*-endothelial migration of leukocytes [62]. The expression of adhesion molecules responsible for leukocyte capture, rolling, adhesion, and transmigration is dependent on the oxidant-sensitive transcription factor NFκB, tightly joining the production of ROS with leukocyte recruitment [63,64].

Our plasma proteomic analysis also revealed several members of the clotting cascade to be significantly upregulated following noise exposure, further supporting our data regarding leukocyte visualization and cerebral vessel function. Fibrinogen (Fgg, Fga) is acute phase reactant and is particularly affected by the acute phase response [45]. Other upregulated factors of the cascade include the factor XIII A chain (F13a1), factor 5 (F5), and factor 10 (F10), which could indicate that pro-thrombotic pathways are active following noise exposure either due to damage of the endothelium, induction of a pro-inflammatory endothelial phenotype, or scavenging of nitric oxide by ROS. Disturbed NO signaling in the microvessels does appear to be an important mechanism that influences platelet function and thrombus formation [65], as NO donors dose-dependently inhibited thrombus formation in rat cerebral vessels [66], and SOD and catalase were reported to reduce the growth of thrombi in the rat mesentery [67]. Even as long ago as in 1982, DMSO and glycerol had been shown to reduce platelet aggregation in pial arteries of mice through hydroxyl radical scavenging [68]. While we cannot presently determine the exact mechanism by which the pro-thrombotic pathways are activated, these mechanisms present an important bridge between the functional and visual studies of the microvessels and the proteomic data within the plasma. We also observed similar effects in humans exposed to nocturnal train noise, resulting in macrovascular endothelial dysfunction and a pro-thrombo-inflammatory phenotype of the plasma proteome [17].

We identified significant upregulation of several proteomic clusters in the plasma of noise-exposed mice, but no notable clusters of down-regulation. The most consequential cluster was related to the induction of acute-phase response: a low-specificity innate immune response to infection, tissue injury, or other disturbances in physiological

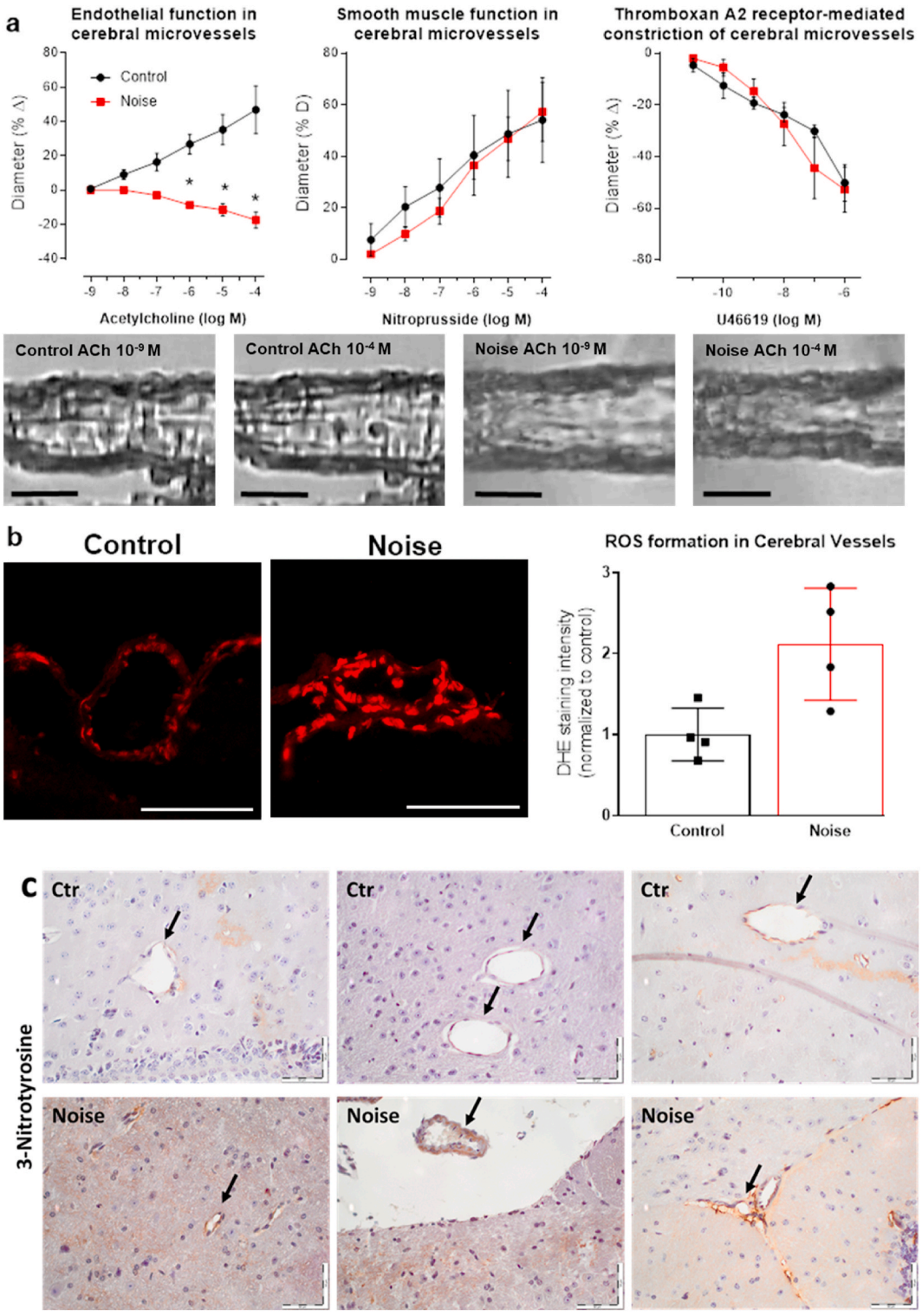

Fig. 8. Noise-induced impairment of vasodilation and oxidative stress in the cerebral microvasculature. (a) In cerebral microvessels, noise caused a marked degree of endothelial dysfunction (impaired ACh-response), while responses to the endothelium independent vasodilator nitroprusside and to the vasoconstrictor U46619 (thromboxane A2 agonist) remained unchanged. Representative pressure myograph microscope images are shown for control and noise exposed cerebral microvessels at low and high ACh concentrations (scale bars correspond to 30 μm). (b) DHE staining revealed an increase in ROS production in cerebral microvessels upon exposure to noise. Representative images of DHE-stained microvascular cryosections are shown besides the densitometric quantification (scale bars correspond to 30 μm). (c) Noise induced a more pronounced staining of 3-nitrotyrosine-positive proteins in microvessels of the brain. 3 representative images per group are shown (n = 6 mice per group in total). Arrows indicate the microvessels and scale bars correspond to 50 μm. Data are the mean ± SD of measurements from 4 individual animals; 2-way ANOVA with Bonferroni's multiple comparison test (a); unpaired *t*-test (b). *P < 0.05 vs. Control.

homeostasis [45]. Importantly, this immunological response is clearly mediated by higher levels of interleukin 6 [69–71], which we have previously demonstrated to be important in our translational model in the brain [44] and plasma [15]. More specifically, the initiation of the complement cascade begins with release of C-reactive protein (CRP) from the liver in response to interleukin-6 levels, which then activates the complement system via C1 precursors [72,73]. Our proteomic analysis reveals induction of C1f, C8b, C8g, and C9, indicating biological responses for microbial targeting, cytokine production, and leukocyte homing. Importantly, the SAPALDIA study of 1389 adults also found significant enrichment of DNA methylation for CRP in response to aircraft and road noise exposures [74], which supports our reported findings of complement involvement in our translational model.

Similarly, serum amyloid A1 and A4 (SAA1/4) are also acute phase reactants. SAA1, specifically, has important roles in lipid metabolism and HDL remodeling following phase response (for review, see Ref. [75]). Further, we assessed oxidative alterations in the lipidome of noise-exposed mice that could represent risk factors and contribute to the development and exacerbation of cardiovascular disease. While we did not find any changes in saturated lipids, we found a significant reduction in the abundance of 16:1 fatty acids and a reduction of 18:1 fatty acids by trend, a consequence of lipid peroxidation initiated by ROS. Supplementation of monounsaturated fatty acids has been shown to improve xanthine oxidase and catalase activity in obese mice [76] and in humans, it is suggested that the reduction in level of biologically active monounsaturated and polyunsaturated fatty acids was caused by the formation of malondialdehyde and of leukocyte-platelet aggregates [77]. Accordingly, incorporation of oleic acid, an 18:1 fatty acid, eicosapentanoic and docosahecaenoic acid (polyunsaturated fatty acids) into the high fat diet of Wistar rats was found to protect against oxidative and inflammatory damage of the retinal microvessels [78].

5. Conclusions

We present novel data on the effects of aircraft noise exposure on the plasma proteome, lipidome, cerebral microvascular function, and leukocytic recruitment to microvessels. It appears that the innate immune-derived ROS that are considered a hallmark of noise-induced stress have a strong impact on the resistance vessels and the well-characterized conductance vessels, as microvascular dysfunction by noise was improved in Nox2 (gp91phox) knockout mice. The oxidative stress appears to either trigger or derive from an acute phase response, resulting in leukocyte recruitment into the endothelium, with possible platelet involvement, and a reduction in levels of antioxidant and anti-inflammatory fatty acids, all of which was mostly normalized in gp91phox$^{-/y}$ mice. The acute phase response appears to influence the clotting cascade as well as endothelial function, priming these vessels for the development of disease. In summary, the increased superoxide formation may impair the vasodilatory action of NO leading to vasoconstriction, which is compatible with the reduced vessel diameter by trend as well as higher 3-nitrotyrosine levels in cerebral microvessels in the noise exposed mice. Of note, a reduced microvessel diameter (increased microvascular resistance) leads to a reduced blood flow, as shown here by reduced red blood cell velocity or segmental blood flow, and in the extreme condition to a stasis [79]. In addition, impairment of NO signaling increases the number of activated platelets and contributes to endothelial activation, all of which will lead to adhesion of platelets and leukocytes to the endothelium (observed here by video microscopy upon rhodamine labeling of leukocytes and markers of thrombo-inflammation in the plasma proteome). The latter will largely increase blood viscosity, prevent red blood cells from sliding on the endothelial surface layer like “skiing on powder snow” [80], all of which explains the reduced blood flow as well as red blood cell velocity observed in the noise exposed mice.

Funding

The work was supported by research grants from the Boehringer Ingelheim Foundation for the collaborative research group ‘Novel and neglected cardiovascular risk factors: molecular mechanisms and therapeutic implications’ to study the effects of aircraft noise exposure on vascular function and oxidative stress (to A.D., S.S., and T.M.). A vascular biology research grant from the Else-Kröner-Fresenius Foundation for “Noise and arterial hypertension” (2017_A10) was awarded to S.S. Katie Frenis, Maria Teresa Bayo Jimenez and Marin Kuntic hold PhD stipends of the TransMed PhD Program at the University Medical Center Mainz. The authors acknowledge the continuous support by the Foundation Heart of Mainz, the Center for Translational Vascular Biology (CTVB) of the University Medical Center Mainz and the DZHK (German Center for Cardiovascular Research), Partner Site Rhine-Main, Mainz, Germany (T.M. is PI of the DZHK). Also financial support by Cancer Research UK (CRUK Edinburgh Centre C157/A255140) and Wellcome Trust (Multiuser Equipment Grant, 208402/Z/17/Z) is gratefully acknowledged.

Declaration of competing interest

The authors declare that they have no competing interests in connection with this manuscript.

Acknowledgements

We are indebted to Angelica Karpi and Nicole Glas for expert technical assistance.

Appendix A. Supplementary data

Supplementary data to this article can be found online at https://doi.org/10.1016/j.redox.2021.102063.

References

[1] E.V. Kempen, M. Casas, G. Pershagen, M. Foraster, WHO environmental noise guidelines for the European region: a systematic review on environmental noise and cardiovascular and metabolic effects: a summary, Int. J. Environ. Res. Publ. Health 15 (2018) 379, https://doi.org/10.3390/ijerph15020379.

[2] WHO report: ENVIRONMENTAL NOISE GUIDELINES for the European Region. http://www.euro.who.int/_data/assets/pdf_file/0008/383921/noise-guidelines-eng.pdf?ua=1, 2018.

[3] L. Fritschi, A.L. Brown, A. Kim, D.H. Schwela, S. Kephalopoulos, WHO and JRC report: burden of disease from environmental noise. https://ec.europa.eu/jrc/sites/jrcsh/files/e94888.pdf, 2011.

[4] D. Vienneau, L. Perez, C. Schindler, C. Lieb, H. Sommer, N. Probst-Hensch, N. Kunzli, M. Roosli, Years of life lost and morbidity cases attributable to transportation noise and air pollution: a comparative health risk assessment for Switzerland in 2010, Int. J. Hyg Environ. Health 218 (2015) 514–521, https://doi.org/10.1016/j.ijheh.2015.05.003.

[5] T. Munzel, S. Kroller-Schon, M. Oelze, T. Gori, F.P. Schmidt, S. Steven, O. Hahad, M. Roosli, J.M. Wunderli, A. Daiber, M. Sorensen, Adverse cardiovascular effects of traffic noise with a focus on nighttime noise and the new WHO noise guidelines, Annu. Rev. Publ. Health 41 (2020) 309–328, https://doi.org/10.1146/annurev-publhealth-081519-062400.

[6] T. Munzel, F.P. Schmidt, S. Steven, J. Herzog, A. Daiber, M. Sorensen, Environmental noise and the cardiovascular system, J. Am. Coll. Cardiol. 71 (2018) 688–697, https://doi.org/10.1016/j.jacc.2017.12.015.

[7] M. Foraster, I.C. Eze, E. Schaffner, D. Vienneau, H. Heritier, S. Endes, F. Rudzik, L. Thiesse, R. Pieren, C. Schindler, A. Schmidt-Trucksass, M. Brink, C. Cajochen, J. Marc Wunderli, M. Roosli, N. Probst-Hensch, Exposure to road, railway, and aircraft noise and arterial stiffness in the SAPALDIA study: annual average noise levels and temporal noise characteristics, Environ. Health Perspect. 125 (2017), https://doi.org/10.1289/EHP1136, 097004.

[8] F.P. Schmidt, M. Basner, G. Kroger, S. Weck, B. Schnorbus, A. Muttray, M. Sariyar, H. Binder, T. Gori, A. Warnholtz, T. Munzel, Effect of nighttime aircraft noise exposure on endothelial function and stress hormone release in healthy adults, Eur. Heart J. 34 (2013) 3508–3514a, https://doi.org/10.1093/eurheartj/eht269.

[9] A. Daiber, S. Steven, A. Weber, V.V. Shuvaev, V.R. Muzykantov, I. Laher, H. Li, S. Lamas, T. Munzel, Targeting vascular (endothelial) dysfunction, Br. J. Pharmacol. 174 (2017) 1591–1619, https://doi.org/10.1111/bph.13517.

[10] W. Babisch, The noise/stress concept, risk assessment and research needs, Noise Health 4 (2002) 1–11.

[11] W. Babisch, Stress hormones in the research on cardiovascular effects of noise, Noise Health 5 (2003) 1–11.
[12] J. Selander, G. Bluhm, T. Theorell, G. Pershagen, W. Babisch, I. Seiffert, D. Houthuijs, O. Breugelmans, F. Vigna-Taglianti, M.C. Antoniotti, E. Velonakis, E. Davou, M.L. Dudley, L. Jarup, H. Consortium, Saliva cortisol and exposure to aircraft noise in six European countries, Environ. Health Perspect. 117 (2009) 1713–1717, https://doi.org/10.1289/ehp.0900933.
[13] A. Daiber, S. Kroller-Schon, K. Frenis, M. Oelze, S. Kalinovic, K. Vujacic-Mirski, M. Kuntic, M.T. Bayo Jimenez, J. Helmstadter, S. Steven, B. Korac, T. Munzel, Environmental noise induces the release of stress hormones and inflammatory signaling molecules leading to oxidative stress and vascular dysfunction-Signatures of the internal exposome, Biofactors 45 (2019) 495–506, https://doi.org/10.1002/biof.1506.
[14] T. Munzel, A. Daiber, S. Steven, L.P. Tran, E. Ullmann, S. Kossmann, F.P. Schmidt, M. Oelze, N. Xia, H. Li, A. Pinto, P. Wild, K. Pies, E.R. Schmidt, S. Rapp, S. Kroller-Schon, Effects of noise on vascular function, oxidative stress, and inflammation: mechanistic insight from studies in mice, Eur. Heart J. 38 (2017) 2838–2849, https://doi.org/10.1093/eurheartj/ehx081.
[15] S. Kroller-Schon, A. Daiber, S. Steven, M. Oelze, K. Frenis, S. Kalinovic, A. Heimann, F.P. Schmidt, A. Pinto, M. Kvandova, K. Vujacic-Mirski, K. Filippou, M. Dudek, M. Bosmann, M. Klein, T. Bopp, O. Hahad, P.S. Wild, K. Frauenknecht, A. Methner, E.R. Schmidt, S. Rapp, H. Mollnau, T. Munzel, Crucial role for Nox2 and sleep deprivation in aircraft noise-induced vascular and cerebral oxidative stress, inflammation, and gene regulation, Eur. Heart J. 39 (2018) 3528–3539, https://doi.org/10.1093/eurheartj/ehy333.
[16] C.C. Wu, S.J. Chen, M.H. Yen, Effects of noise on blood pressure and vascular reactivities, Clin. Exp. Pharmacol. Physiol. 19 (1992) 833–838.
[17] J. Herzog, F.P. Schmidt, O. Hahad, S.H. Mahmoudpour, A.K. Mangold, P. Garcia Andreo, J. Prochaska, T. Koeck, P.S. Wild, M. Sorensen, A. Daiber, T. Munzel, Acute exposure to nocturnal train noise induces endothelial dysfunction and pro-thromboinflammatory changes of the plasma proteome in healthy subjects, Basic Res. Cardiol. 114 (2019) 46, https://doi.org/10.1007/s00395-019-0753-y.
[18] C.C. Wu, S.J. Chen, M.H. Yen, Attenuation of endothelium-dependent relaxation in mesenteric artery during noise-induced hypertension, J. Biomed. Sci. 1 (1994) 49–53.
[19] W.S. Quirk, M.D. Seidman, Cochlear vascular changes in response to loud noise, Am. J. Otol. 16 (1995) 322–325.
[20] E.A. Peterson, J.S. Augenstein, D.C. Tanis, D.G. Augenstein, Noise raises blood pressure without impairing auditory sensitivity, Science 211 (1981) 1450–1452.
[21] A.L. Baldwin, I.R. Bell, Effect of noise on microvascular integrity in laboratory rats, J Am Assoc Lab Anim Sci 46 (2007) 58–65.
[22] M.W. Laschke, B. Vollmar, M.D. Menger, The dorsal skinfold chamber: window into the dynamic interaction of biomaterials with their surrounding host tissue, Eur. Cell. Mater. 22 (2011) 147–164, discussion 164-147.
[23] J. Rappsilber, Y. Ishihama, M. Mann, Stop and go extraction tips for matrix-assisted laser desorption/ionization, nanoelectrospray, and LC/MS sample pretreatment in proteomics, Anal. Chem. 75 (2003) 663–670, https://doi.org/10.1021/ac026117i.
[24] Y. Wang, F. Yang, M.A. Gritsenko, Y. Wang, T. Clauss, T. Liu, Y. Shen, M. E. Monroe, D. Lopez-Ferrer, T. Reno, R.J. Moore, R.L. Klemke, D.G. Camp 2nd, R. D. Smith, Reversed-phase chromatography with multiple fraction concatenation strategy for proteome profiling of human MCF10A cells, Proteomics 11 (2011) 2019–2026, https://doi.org/10.1002/pmic.201000722.
[25] J. Cox, N. Neuhauser, A. Michalski, R.A. Scheltema, J.V. Olsen, M. Mann Andromeda, A peptide search engine integrated into the MaxQuant environment, J. Proteome Res. 10 (2011) 1794–1805, https://doi.org/10.1021/pr101065j.
[26] S. Tyanova, T. Temu, P. Sinitcyn, A. Carlson, M.Y. Hein, T. Geiger, M. Mann, J. Cox, The Perseus computational platform for comprehensive analysis of (prote) omics data, Nat. Methods 13 (2016) 731–740, https://doi.org/10.1038/nmeth.3901.
[27] P. Shannon, A. Markiel, O. Ozier, N.S. Baliga, J.T. Wang, D. Ramage, N. Amin, B. Schwikowski, T. Ideker, Cytoscape: a software environment for integrated models of biomolecular interaction networks, Genome Res. 13 (2003) 2498–2504, https://doi.org/10.1101/gr.1239303.
[28] J. Muntel, T. Gandhi, L. Verbeke, O.M. Bernhardt, T. Treiber, R. Bruderer, L. Reiter, Surpassing 10 000 identified and quantified proteins in a single run by optimizing current LC-MS instrumentation and data analysis strategy, Mol Omics 15 (2019) 348–360, https://doi.org/10.1039/c9mo00082h.
[29] M.H. Sarafian, M. Gaudin, M.R. Lewis, F.P. Martin, E. Holmes, J.K. Nicholson, M. E. Dumas, Objective set of criteria for optimization of sample preparation procedures for ultra-high throughput untargeted blood plasma lipid profiling by ultra performance liquid chromatography-mass spectrometry, Anal. Chem. 86 (2014) 5766–5774, https://doi.org/10.1021/ac500317c.
[30] A.J. Chetwynd, W.B. Dunn, G. Rodriguez-Blanco, Collection and preparation of clinical samples for metabolomics, Adv. Exp. Med. Biol. 965 (2017) 19–44, https://doi.org/10.1007/978-3-319-47656-8_2.
[31] G.M. Mackay, L. Zheng, N.J. van den Broek, E. Gottlieb, Analysis of cell metabolism using LC-MS and isotope tracers, Methods Enzymol. 561 (2015) 171–196, https://doi.org/10.1016/bs.mie.2015.05.016.
[32] N. Danne-Rasche, C. Coman, R. Ahrends, Nano-LC/NSI MS refines lipidomics by enhancing lipid coverage, measurement sensitivity, and linear dynamic range, Anal. Chem. 90 (2018) 8093–8101, https://doi.org/10.1021/acs.analchem.8b01275.
[33] C.A. Smith, E.J. Want, G. O'Maille, R. Abagyan, G. Siuzdak, XCMS: processing mass spectrometry data for metabolite profiling using nonlinear peak alignment, matching, and identification, Anal. Chem. 78 (2006) 779–787, https://doi.org/10.1021/ac051437y.
[34] S. Li, Y. Park, S. Duraisingham, F.H. Strobel, N. Khan, Q.A. Soltow, D.P. Jones, B. Pulendran, Predicting network activity from high throughput metabolomics, PLoS Comput. Biol. 9 (2013), https://doi.org/10.1371/journal.pcbi.1003123 e1003123.
[35] L. Goracci, S. Tortorella, P. Tiberi, R.M. Pellegrino, A. Di Veroli, A. Valeri, G. Cruciani, Lipostar, a comprehensive platform-neutral cheminformatics tool for lipidomics, Anal. Chem. 89 (2017) 6257–6264, https://doi.org/10.1021/acs.analchem.7b01259.
[36] P.D. Hutchins, J.D. Russell, J.J. Coon LipiDex, An integrated software package for high-confidence lipid identification, Cell Syst 6 (2018) 621–625, https://doi.org/10.1016/j.cels.2018.03.011, e625.
[37] C.A. Reichel, M.E. Hessenauer, K. Pflieger, M. Rehberg, S.M. Kanse, S. Zahler, F. Krombach, A. Berghaus, S. Strieth, Components of the plasminogen activation system promote engraftment of porous polyethylene biomaterial via common and distinct effects, PloS One 10 (2015), https://doi.org/10.1371/journal.pone.0116883 e0116883.
[38] M. Baker, H. Wayland, On-line volume flow rate and velocity profile measurement for blood in microvessels, Microvasc. Res. 7 (1974) 131–143, https://doi.org/10.1016/0026-2862(74)90043-0.
[39] A. Gericke, J.J. Sniatecki, E. Goloborodko, A. Steege, O. Zavaritskaya, J.M. Vetter, F.H. Grus, A. Patzak, J. Wess, N. Pfeiffer, Identification of the muscarinic acetylcholine receptor subtype mediating cholinergic vasodilation in murine retinal arterioles, Invest. Ophthalmol. Vis. Sci. 52 (2011) 7479–7484, https://doi.org/10.1167/iovs.11-7370.
[40] A. Gericke, E. Goloborodko, N. Pfeiffer, C. Manicam, Preparation steps for measurement of reactivity in mouse retinal arterioles ex vivo, JoVE (2018), https://doi.org/10.3791/56199.
[41] K. Frenis, J. Helmstadter, Y. Ruan, E. Schramm, S. Kalinovic, S. Kroller-Schon, M. T. Bayo Jimenez, O. Hahad, M. Oelze, S. Jiang, P. Wenzel, C.J. Sommer, K.B. M. Frauenknecht, A. Waisman, A. Gericke, A. Daiber, T. Munzel, S. Steven, Ablation of lysozyme M-positive cells prevents aircraft noise-induced vascular damage without improving cerebral side effects, Basic Res. Cardiol. 116 (2021) 31, https://doi.org/10.1007/s00395-021-00869-5.
[42] J.K. Zadeh, M.B. Zhutdieva, P. Laspas, C. Yuksel, A. Musayeva, N. Pfeiffer, C. Brochhausen, M. Oelze, A. Daiber, N. Xia, H. Li, A. Gericke, Apolipoprotein E deficiency causes endothelial dysfunction in the mouse retina, Oxidative medicine and cellular longevity 2019 (2019) 5181429, https://doi.org/10.1155/2019/5181429.
[43] A. Gericke, C. Mann, J.K. Zadeh, A. Musayeva, I. Wolff, M. Wang, N. Pfeiffer, A. Daiber, H. Li, N. Xia, V. Prokosch, Elevated intraocular pressure causes abnormal reactivity of mouse retinal arterioles. Oxidative medicine and cellular longevity 2019. https://doi.org/10.1155/2019/9736047, 2019, 9736047.
[44] S. Steven, K. Frenis, S. Kalinovic, M. Kvandova, M. Oelze, J. Helmstadter, O. Hahad, K. Filippou, K. Kus, C. Trevisan, K.D. Schluter, K. Boengler, S. Chlopicki, K. Frauenknecht, R. Schulz, M. Sorensen, A. Daiber, S. Kroller-Schon, T. Munzel, Exacerbation of adverse cardiovascular effects of aircraft noise in an animal model of arterial hypertension, Redox biology 34 (2020) 101515, https://doi.org/10.1016/j.redox.2020.101515.
[45] E. Gruys, M.J. Toussaint, T.A. Niewold, S.J. Koopmans, Acute phase reaction and acute phase proteins, J. Zhejiang Univ. - Sci. B 6 (2005) 1045–1056, https://doi.org/10.1631/jzus.2005.B1045.
[46] E. Piktel, I. Levental, B. Durnas, P.A. Janmey, R. Bucki, Plasma gelsolin: indicator of inflammation and its potential as a diagnostic tool and therapeutic target, Int. J. Mol. Sci. 19 (2018), https://doi.org/10.3390/ijms19092516.
[47] M. Katayama, S. Hirai, K. Kamihagi, K. Nakagawa, M. Yasumoto, I. Kato, Soluble E-cadherin fragments increased in circulation of cancer patients, Br. J. Canc. 69 (1994) 580–585, https://doi.org/10.1038/bjc.1994.106.
[48] C. Chang, B.L. Worley, R. Phaeton, N. Hempel, Extracellular glutathione peroxidase GPx3 and its role in cancer, Cancers 12 (2020), https://doi.org/10.3390/cancers12082197.
[49] L.O. Chaves, J.C.C. Carraro, F.C. Vidigal, J. Bressan, Higher waist circumference is related to lower plasma polyunsaturated fatty acids in healthy participants: metabolic implications, J. Am. Coll. Nutr. 38 (2019) 342–350, https://doi.org/10.1080/07315724.2018.1518171.
[50] J. Assies, R.J. Mocking, A. Lok, H.G. Ruhe, F. Pouwer, A.H. Schene, Effects of oxidative stress on fatty acid- and one-carbon-metabolism in psychiatric and cardiovascular disease comorbidity, Acta Psychiatr. Scand. 130 (2014) 163–180, https://doi.org/10.1111/acps.12265.
[51] W. Babisch, Updated exposure-response relationship between road traffic noise and coronary heart diseases: a meta-analysis, Noise Health 16 (2014) 1–9, https://doi.org/10.4103/1463-1741.127847.
[52] M.T. Osborne, A. Radfar, M.Z.O. Hassan, S. Abohashem, B. Oberfeld, T. Patrich, B. Tung, Y. Wang, A. Ishai, J.A. Scott, L.M. Shin, Z.A. Fayad, K.C. Koenen, S. Rajagopalan, R.K. Pitman, A. Tawakol, A neurobiological mechanism linking transportation noise to cardiovascular disease in humans, Eur. Heart J. 41 (2020) 772–782, https://doi.org/10.1093/eurheartj/ehz820.
[53] A. Recio, C. Linares, J.R. Banegas, J. Diaz, Road traffic noise effects on cardiovascular, respiratory, and metabolic health: an integrative model of biological mechanisms, Environ. Res. 146 (2016) 359–370, https://doi.org/10.1016/j.envres.2015.12.036.
[54] W. Schulte, G. Heusch, A.W. von Eiff, [The influence of experimental traffic noise on autonomous functions of normotensives and hypertensives after stress (author's transl)], Basic Res. Cardiol. 72 (1977) 575–583, https://doi.org/10.1007/BF01907038.

[55] T. Munzel, T. Gori, W. Babisch, M. Basner, Cardiovascular effects of environmental noise exposure, Eur. Heart J. 35 (2014) 829–836, https://doi.org/10.1093/eurheartj/ehu030.
[56] F. Schmidt, K. Kolle, K. Kreuder, B. Schnorbus, P. Wild, M. Hechtner, H. Binder, T. Gori, T. Munzel, Nighttime aircraft noise impairs endothelial function and increases blood pressure in patients with or at high risk for coronary artery disease, Clin. Res. Cardiol. 104 (2015) 23–30, https://doi.org/10.1007/s00392-014-0751-x.
[57] P.L. Ludmer, A.P. Selwyn, T.L. Shook, R.R. Wayne, G.H. Mudge, R.W. Alexander, P. Ganz, Paradoxical vasoconstriction induced by acetylcholine in atherosclerotic coronary arteries, N. Engl. J. Med. 315 (1986) 1046–1051, https://doi.org/10.1056/NEJM198610233151702.
[58] T. Heitzer, T. Schlinzig, K. Krohn, T. Meinertz, T. Munzel, Endothelial dysfunction, oxidative stress, and risk of cardiovascular events in patients with coronary artery disease, Circulation 104 (2001) 2673–2678, https://doi.org/10.1161/hc4601.099485.
[59] S. Rajagopalan, S. Kurz, T. Munzel, M. Tarpey, B.A. Freeman, K.K. Griendling, D. G. Harrison, Angiotensin II-mediated hypertension in the rat increases vascular superoxide production via membrane NADH/NADPH oxidase activation. Contribution to alterations of vasomotor tone, J. Clin. Invest. 97 (1996) 1916–1923, https://doi.org/10.1172/JCI118623.
[60] A. Warnholtz, G. Nickenig, E. Schulz, R. Macharzina, J.H. Brasen, M. Skatchkov, T. Heitzer, J.P. Stasch, K.K. Griendling, D.G. Harrison, M. Bohm, T. Meinertz, T. Munzel, Increased NADH-oxidase-mediated superoxide production in the early stages of atherosclerosis: evidence for involvement of the renin-angiotensin system, Circulation 99 (1999) 2027–2033, https://doi.org/10.1161/01.cir.99.15.2027.
[61] G. Heusch, Coronary microvascular obstruction: the new frontier in cardioprotection, Basic Res. Cardiol. 114 (2019) 45, https://doi.org/10.1007/s00395-019-0756-8.
[62] H.F. Langer, T. Chavakis, Leukocyte-endothelial interactions in inflammation, J. Cell Mol. Med. 13 (2009) 1211–1220, https://doi.org/10.1111/j.1582-4934.2009.00811.x.
[63] D.N. Granger, P. Kubes, The microcirculation and inflammation: modulation of leukocyte-endothelial cell adhesion, J. Leukoc. Biol. 55 (1994) 662–675.
[64] J. Panes, D.N. Granger, Leukocyte-endothelial cell interactions: molecular mechanisms and implications in gastrointestinal disease, Gastroenterology 114 (1998) 1066–1090, https://doi.org/10.1016/s0016-5085(98)70328-2.
[65] J.E. Freedman, Oxidative stress and platelets, Arterioscler. Thromb. Vasc. Biol. 28 (2008) s11–16, https://doi.org/10.1161/ATVBAHA.107.159178.
[66] Y. Sasaki, J. Seki, J.C. Giddings, J. Yamamoto, Effects of NO-donors on thrombus formation and microcirculation in cerebral vessels of the rat, Thromb. Haemostasis 76 (1996) 111–117.
[67] M.A. Peire, P. Puig-Parellada, Oxygen-free radicals and nitric oxide are involved in the thrombus growth produced by iontophoresis of ADP, Pharmacol. Res. 38 (1998) 353–356, https://doi.org/10.1006/phrs.1998.0372.
[68] W.I. Rosenblum, F. El-Sabban, Dimethyl sulfoxide (DMSO) and glycerol, hydroxyl radical scavengers, impair platelet aggregation within and eliminate the accompanying vasodilation of, injured mouse pial arterioles, Stroke; a journal of cerebral circulation 13 (1982) 35–39, https://doi.org/10.1161/01.str.13.1.35.
[69] P.C. Heinrich, I. Behrmann, G. Muller-Newen, F. Schaper, L. Graeve, Interleukin-6-type cytokine signalling through the gp130/Jak/STAT pathway, Biochem. J. 334 (Pt 2) (1998) 297–314, https://doi.org/10.1042/bj3340297.
[70] A. Koj, Regulation of the acute phase and immune responses: interleukin-6, Ann. N. Y. Acad. Sci. 557 (1989) 1–583.
[71] J.M. Le, J. Vilcek, Interleukin 6: a multifunctional cytokine regulating immune reactions and the acute phase protein response, Laboratory investigation; a journal of technical methods and pathology 61 (1989) 588–602.
[72] M. Del Giudice, S.W. Gangestad, Rethinking IL-6 and CRP: why they are more than inflammatory biomarkers, and why it matters, Brain Behav. Immun. 70 (2018) 61–75, https://doi.org/10.1016/j.bbi.2018.02.013.
[73] N. Nishimoto, K. Terao, T. Mima, H. Nakahara, N. Takagi, T. Kakehi, Mechanisms and pathologic significances in increase in serum interleukin-6 (IL-6) and soluble IL-6 receptor after administration of an anti-IL-6 receptor antibody, tocilizumab, in patients with rheumatoid arthritis and Castleman disease, Blood 112 (2008) 3959–3964, https://doi.org/10.1182/blood-2008-05-155846.
[74] I.C. Eze, A. Jeong, E. Schaffner, F.I. Rezwan, A. Ghantous, M. Foraster, D. Vienneau, F. Kronenberg, Z. Herceg, P. Vineis, M. Brink, J.M. Wunderli, C. Schindler, C. Cajochen, M. Roosli, J.W. Holloway, M. Imboden, N. Probst-Hensch, Genome-wide DNA methylation in peripheral blood and long-term exposure to source-specific transportation noise and air pollution: the SAPALDIA study, Environ. Health Perspect. 128 (2020) 67003, https://doi.org/10.1289/EHP6174.
[75] L. Sun, R.D. Ye, Serum amyloid A1: structure, function and gene polymorphism, Gene 583 (2016) 48–57, https://doi.org/10.1016/j.gene.2016.02.044.
[76] C. Hunsche, O. Hernandez, A. Gheorghe, L.E. Diaz, A. Marcos, M. De la Fuente, Immune dysfunction and increased oxidative stress state in diet-induced obese mice are reverted by nutritional supplementation with monounsaturated and n-3 polyunsaturated fatty acids, Eur. J. Nutr. 57 (2018) 1123–1135, https://doi.org/10.1007/s00394-017-1395-1.
[77] I. Bikulciene, O. Golubevaite, V. Zekas, M. Radzevicius, D. Karciauskaite, R. Matuzeviciene, V. Hendrixson, A. Mazeikiene, N. Burokiene, A. Kaminskas, Z. A. Kucinskiene, Association of platelet membrane fatty acid composition with markers of oxidative stress in healthy men, Med. Sci. Mon. Int. Med. J. Exp. Clin. Res. : international medical journal of experimental and clinical research 25 (2019) 6405–6416, https://doi.org/10.12659/MSM.915111.
[78] S. Bettadahalli, P. Acharya, R. Talahalli, Evidence on n-3 fatty acids and oleic acid role in retinal inflammation and microvascular integrity: insight from a hyperlipidemic rat model, Inflammation 43 (2020) 868–877, https://doi.org/10.1007/s10753-019-01172-1.
[79] G. Guven, M.P. Hilty, C. Ince, Microcirculation: physiology, pathophysiology, and clinical application, Blood Purif. 49 (2020) 143–150, https://doi.org/10.1159/000503775.
[80] T.W. Secomb, Blood flow in the microcirculation, Annu. Rev. Fluid Mech. 49 (2017) 443–461, https://doi.org/10.1146/annurev-fluid-010816-060302.